Mechanochemical synthesis of nanostructured metal nitrides, carbonitrides and carbon nitride: A combined theoretical and experimental study
Peer-reviewed author version

Mechanochemical reaction of metallic elements and melamine: A facile and versatile synthetic approach towards nanostructured metal nitrides, carbonitrides and carbon nitride

Mechanochemical reaction of metallic elements and melamine: A combined theoretical and experimental study

Mechanochemical synthesis of nanostructured metal nitrides, carbonitrides and carbon nitride: A combined theoretical and experimental study

Seyyed Amin Rounaghi[1,*], Danny E. P. Vanpoucke[2], Hossein Eshghi[3], Sergio Scudino[4], Elaheh Esmaeili[5], Steffen Oswald[4], Jürgen Eckert[6,7]

1) Department of Materials Engineering, Birjand University of Technology, Birjand, Iran.

2) UHasselt, Institute for Materials Research (IMO-IMOMEC), Agoralaan, 3590 Diepenbeek, Belgium.

3) Department of Chemistry, Faculty of Sciences, Ferdowsi University of Mashhad, 91775-1436 Mashhad, Iran.

4) Institut für Komplexe Materialien, IFW Dresden, 01069 Dresden, Germany.

5) Department of Chemical Engineering, Birjand University of Technology, Birjand, Iran.

6) Erich Schmid Institute of Materials Science, Austrian Academy of Sciences, Jahnstraße 12, A-8700 Leoben, Austria

7) Department Materials Physics, Montanuniversität Leoben, Jahnstraße 12, A-8700 Leoben, Austria

*Corresponding author. E-mail address: *rounaghi@birjandut.ac.ir*

Abstract

Nowadays, development of highly efficient routes for the facile and low cost synthesis of new generation of materials is greatly growing. Nitrides are one of those promising materials which are traditionally prepared by the carbothermal reduction of metal oxides at high temperatures in the exposure of the toxic ammonia atmosphere. In the present study, we describe a versatile, facile and low cost mechanochemical process for the synthesis of nanostructured metal nitrides (MNs), carbonitrides (MCNs) and carbon nitride (CN_x). Based on this technique, melamine as a solid nitrogen-containing organic compound (SNCOC) is ball milled with four distinct metal powders including Al, Ti, Cr and V elements to produce nanostructured AlN, TiC_xN_{1-x}, CrC_xN_{1-x}, and VC_xN_{1-x} ($x \sim 0.05$). Both theoretical and experimental techniques are implemented to determine the reaction intermediates, products, by-products and finally, the mechanism underling this synthetic route. According to the results, melamine is polymerized in the presence of metallic elements at intermediate stages of the milling process, leading to the formation of a carbon nitride network. The CN_x phase, then, react with the metallic precursors to form MN, MCN or even $MCN-CN_x$ nano-composites depend on the thermodynamic stability of corresponding metal nitride and carbide.

1. Introduction

Nitrides have been known as a unique class of the valuable materials due to their potential applications in wide band gap semiconductors (group III nitrides; AlGaN, GaN) [1, 2] refractory ceramics (Si_3N_4 [3]), corrosive and abrasive resistant thin films (CrN,[4] TiN [5]), and catalysts (VN [6], C_3N_4 [7, 8]). Nitrides are traditionally fabricated by direct nitridation of metals or carbothermal reduction of metal oxides under N_2 or NH_3 atmosphere [9, 10]. These processes, however, suffer from the toxic ammonia gas involved and the long time exposure of the reactants at elevated temperatures, which is inevitable for achieving to the full conversion. During the past decade, numerous attempts have been made to reduce the reaction temperature by the implementation of different nitrogen-containing gaseous species. Paseuth and Shimada used an aluminum oleic emulsion for preparation of the nanostructured AlN at moderate temperatures of about 1423-1473 K in NH_3 [11]. They proposed that the reaction of NH_3 with the amorphous carbon structure prepared during decomposition of aluminum oleic forms gaseous HCN species which react with Al_2O_3 and shift the reduction-nitridation process to lower temperatures. The detection of HCN species during the analysis of the gas outlet in other carbothermal reduction systems confirmed that the formation temperature and concentration of these radicals directly affect the temperature and reaction time required for the synthesis of the nitride [12, 13].

An intresting solid-state synthetic route was proposed by Zhao et al. [14] based on which metal nitrides were fabricated through the reaction of metal oxide and solid nitrogen-containing organic compounds (SNCOCs) such as melamine [14], cyanamide [15], dicyanamide [16] or carbon nitride (C_3N_4) at moderate temperatures and in sealed conditions. According to the way they reported, the reaction was started at temperatures above 873 K, in which SNCOCs were decomposed, which in turn resulted to the nitrogen-containing radicals such as C_2N^{+2}, C_3N^{+2}, C_3N^{+3}, C_3N^{+4} and $HCNH^+$ [15]. These active radicals can reduce the

3

metal oxides into the corresponding metallic elements. Therefore, the metal nitrides were prepared by the nitridation of metallic particles with the residual carbon nitride [16].

The mentioned process, although, was successfully employed for the synthesis of a wide range of common nitrides, but, some drawbacks such as toxicity of the gaseous species, high temperature requirements and some difficulties related to the sealed conditions considerably limited the extensive use of this route.

Sol-gel chemistry and in particular, urea glass route is another alternative method which is recently implemented for the synthesis of nanostructured metal nitrides (MNs) or carbonitrides (MCNs) [17]. During this process, first a porous gel is prepared from a sol of metal halides and a CHN-containing organic precursor such as urea. The corresponding MN or MCN, then, is fabricated by heating of the gel at moderate temperatures in a flux of N_2. This method, although benefits from relatively low temperature synthesis without any demands for the sealed conditions, but, the toxicity of involved gases and the necessity for the post thermal treatment still remained as the open issues.

Global demands for the green and low temperature material synthesis support the mechanochemical approach as a unique opportunity for room temperature fabrication of a wide spectrum of nanostructured materials including oxides, hydrides, nitrides and two dimensional materials [18-20] [21, 22]. The activation energy required for the reaction, in this technique, is provided by the mechanical forces usually induced by the ball impacts in a conventional high-energy ball milling [20]. The mechanochemical synthesis of nitrides, so far, has just focused on the solid-gas interactions, such that the metal or metal oxide powder is milled in N_2 or NH_3 atmosphere [23-25]. This process suffers from several shortcomings which include the pressurized N_2 or NH_3 atmosphere and the prolonged milling times requeired for the reaction compeltion due to the inertness of N_2 and poor contacting of the reactants (solid–gas) [23, 25, 26]. Overcoming

these limitations, substitution of the gaseous atmospheres with solid nitrogen rich compounds such as those described as SNCOCs are supposed to enhance contacting of the reactants and therefore accelerate the nitridation reaction. The mentioned claim has been technically investigated on few metal-organic milling systems such as Al-melamine [29], Al-diaminomaleonitrile (DAMN) [30], Ti-urea [31] and Ti-melamine [32]. Nanostructured AlN and TiCN were successfully synthesized during milling, suggesting an inexpensive, safe and versatile mechanochemical process for the synthesis of nanostructured MNs and MCNs. Moreover, the governing mechanism of AlN synthesis in Al-melamine milling system has been reported through a combined theoretical and experimental study [27].

Since, melamine as a safe, nontoxic and inexpensive SNCOC with a high nitrogen content (66.6 wt.%) is a promising candidate for the solid-state nitridation, therefore, this study aims to synthesize various technically important metal nitrides (MNs) and carbonitrides (MCNs) using mechanochemical route. Furthermore, this investigation provides the first principle theoretical and experimental insights into the structure of intermediates, final products and the reaction mechanism involved.

2. Experimental procedure

2-1. sample preparation

Al (Goodfellow, 99.5 % purity), Ti (Alfa Aesar, 99.9 % purity), Cr (Alfa, 99% purity), V (Alfa, 99.5% purity) and melamine (Khorasan Petrochemical Co., 99.8 % purity) were purchased and used as received without further purification. Metallic powders were separately mixed with melamine with stoichiometric ratio of 6:1to get four distinct mixtures of aluminum-melamine (Al-M), titanium-melamine (Ti-M), chromium-melamine (Cr-M) and vanadium- melamine (V-M). About 3 g of each powder mixture was subjected into a hardened steel vial along with the hardened steel balls (10 mm diameter) to obtain a ball-to-

powder weight ratio of 50:1. Vial charging, discharging and all sample handling steps were performed in a purified argon filled glove box with an oxygen and water partial pressures of less than 1 ppm. The milling experiments were conducted at ambient temperature using a Retsch PM-400 planetary ball mill at a rotating speed of 300 rpm. The milling time was considered based on the type of the applied initial powders in the range of 6-84 h. The milling process was ceased at the specific time intervals and a small portion of powders was removed and stored in the glove box for further characterization.

2-2. Materials characterization

X-ray diffraction (XRD) data were collected on a Philips X'Pert X-ray diffractometer with Co Kα radiation ($\lambda = 0.17889$ nm). The Rietveld refining method was used to evaluate the crystallite size of the milled products. Fourier transform infrared (FTIR) spectra were recorded on a ThermoNicolet Avatar 370 infrared spectrometer at room temperature using the KBr pellet technique. Chemical configuration of the powders was determined by the X-ray photoelectron spectroscope (XPS) in an ultra-high vacuum system equipped with a hemispherical electron analyzer (SPECS PHOIBOS 100) at room temperature. The photoelectrons were excited with a non-monochromatic Mg Kα (1253.6 eV) radiation and 300 W power. The energy calibrations were made against the C 1s peak (284.5 eV) to eliminate the charging of the sample during analysis. A Gemini 1530 (Zeiss) microscope supplied by an energy dispersive X-ray spectrometer (EDX) was applied to produce the SEM images.

2-3. DFT calculations

The periodic ab-initio calculations are performed within the Projector Augmented Wave (PAW) method as implemented in VASP code [28, 29]. The kinetic energy cut-off was set to

600 eV and energy-convergence was set to 1.0x10-8 for the total energy. For C and N, the 2s and 2p electrons were considered as valence electrons, while for Al, Ti, V and Cr we considered $2s^2 2p^6 3s^2 3p^1$, $3s^2 3p^6 4s^2 3d^2$, $3p^6 4s^2 3d^3$ and $3p^6 4s^1 3d^5$ as valence electrons, respectively. We used a generalized gradient approximation as defined by Perdew-Burke-Ernzerhof to describe the exchange and correlation behaviour of the electrons [30]. All structures were allowed to fully optimize both atomic positions and lattice parameters. At the end of the relaxation, the largest force found on the atom was below 1 meV/Å (with the exception of some of the Al-based systems). Supercells were created from each of the host materials, to lead to dopant concentrations of about 1-3% at. The symmetry group of each of the host materials is given in the table S1, as are the super-cells used for the doped systems. K-point sets used for the structure relaxation (relax) and final total energy calculation (static) are given as well [31].

Two types of doping were considered: substitutional doping (Sub) and interstitial doping (Int). For the pure metals, a single metal atom of the supercell is replaced by a dopant atom for substitutional doping, while for the nitrides and carbides, the substituted atom is either a N or a C atom, respectively. For systems with multiple interstitial or substitutional positions, the initial positions are shown in the Fig. S1.

3. Results and discussion

The phase evolution of the powder mixtures at various milling times was investigated by XRD analysis, as shown in Figs. S2 a-d. In the patterns, the weak peaks appeared at 30-35 ° are arisen from the sample holder. As observed, at the initial stages of the milling, the corresponding peaks of both the organic and metallic precursors are less intensified. Upon the nitridation reaction starts, the metallic precursors are gradually consumed, supported by the elimination of the metallic peaks and the appearance of the new broad peaks related to the

7

distinct structures of metal nitride and/ or carbonitride. Figure 1 presents the XRD patterns of the final products prepared by the milling of Al-M, Ti-M, Cr-M and V-M powder mixtures for 6, 30, 84 and 30 h, respectively. The patterns are indexed to AlN, TiC_xN_{1-x}, CrC_xN_{1-x} and $VC_xN_{1-x}/V_2C_xN_{1-x}$ as specified by the corresponding diffraction planes. Table 1 provides further crystallographic information of these phases. As seen, each carbonitride phase exhibits a crystallographic structure close to the parent nitride implying on the nitrogen-rich feature of the synthesized carbonitrides. The only exception is found to be occurred in V-M milling system in which two types of vanadium carbonitride is formed i.e. VC_xN_{1-x} and $V_2C_xN_{1-x}$. While VC_xN_{1-x} is a nitrogen rich phase with the parent cubic VN structure (space group Fm3m) but $V_2C_xN_{1-x}$ reveals a structure similar to orthorhombic V_2C (space group Pbcn) and considers as a carbon rich phase.
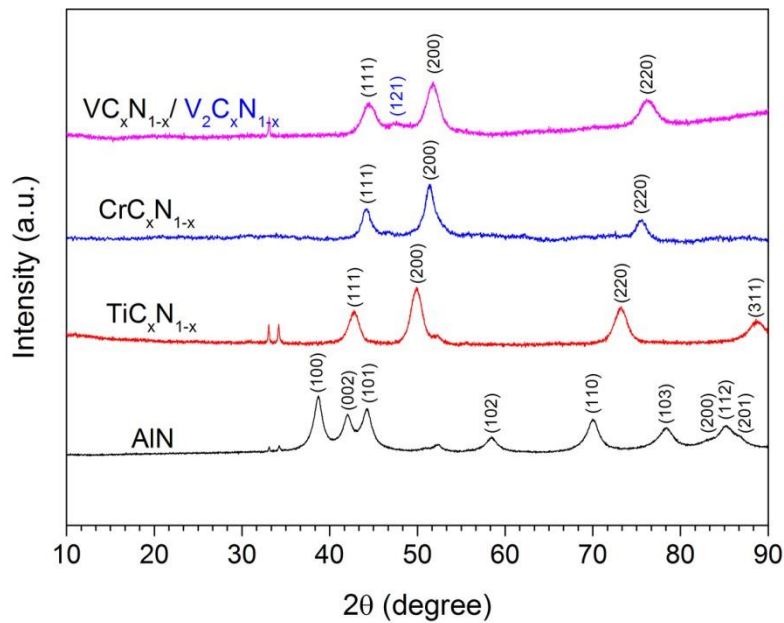

Fig. 1. XRD patterns of Al-M, Ti-M, Cr-M and V-M powder mixtures milled for 6, 30, 84 and 30 h, respectively.

The patterns in Fig. 1 demonstrate significant peak broadening resulted from strain-induced structures and fine crystallite sizes. The crystallite size of the synthesized products was

8

determined by Rietveld refinement method and the results are given in Table 1. As seen, all the synthesized metal nitride/ carbonitride powders show the crystallite sizes in the nanometric scale, ranging from 7 to 11 nm.

Table 1. The crystal structure, space group and crystallite size of the synthesized powders inferred from XRD patterns in Fig. 1.

Metal nitride/Carbonitride	Crystal structure	Space group	Crystallite size (nm)
AlN	Hexagonal	P63mc	11
TiC_xN_{1-x}	Cubic	Fm3m	11
CrC_xN_{1-x}	Cubic	Fm3m	10
VC_xN_{1-x}	Cubic	Fm3m	7
$V_2C_xN_{1-x}$	Orthorhombic	Pbcn	27

FTIR spectra of the synthesized metal nitrides are displayed in Fig. 2. The peaks at 1629 cm^{-1} and 3407 cm^{-1} are assigned to the bending and stretching vibration modes of the hydroxyl group (–OH), resulting from moisture absorption and surface hydrolysis of the nitrides. The broad peaks at the range of 400-1000 cm^{-1} observed for all the spectra are mainly attributed to the formation of the corresponding metal nitrides and carbonitrides. In particular, the strong broad peak centered at about 728 cm^{-1} points to the Al–N bond stretching vibration mode (Fig. 2a) [32]. In Fig. 2b, the broad peak at about 400-960 cm^{-1} is attributed to the combination of several stretching vibration modes related to Ti–C, Ti–N and Ti–O [33-35]. The IR spectrum of CrC_xN_{1-x} illustrates two separately different peaks (Fig. 2c). The first broad peak at 450-720 cm^{-1} is assigned to Cr–N and Cr–C bonds [36] and the weakly second one at around 1045 cm^{-1} is attributed to the Cr–O vibrations [37]. According to the figure 2d, the IR spectrum of $VC_xN_{1-x}/V_2C_xN_{1-x}$ reveals three distinct peaks; The main peak at 940 cm^{-1}

is related to the V–N bond stretching vibration mode [38] and two the others centroid at about 663 and 795 cm^{-1} are respectively, associated with V–O and V–C stretching vibration modes [39, 40].

Therefore, one may rationalize the presence of the MN and MCN in the resulted milling products as a result of the appearance of the M–N and M–C bonds in the above-investigated FTIR spectra. The presence of an oxide layer is also supported by the surface oxidation of the powder particles during sample handling and preparation. The weak peak appeared at around 2100-2200 cm^{-1} in AlN and VC_xN_{1-x} /$V_2C_xN_{1-x}$ spectra (Figs. 2a and d) are mainly explained by C≡N or N=C=N bonds [41], formed as traces in process by-products. Based on what implied in Fig. 2d, a broad and intense peak appeared at the range of 1000-1720 cm^{-1} in the IR spectrum of VC_xN_{1-x} /$V_2C_xN_{1-x}$ sample may be attributed to the CN bonds (C–N and C=N) in a nitrogen-containing carbonaceous material with C/N aromatic ring structure [42, 43].
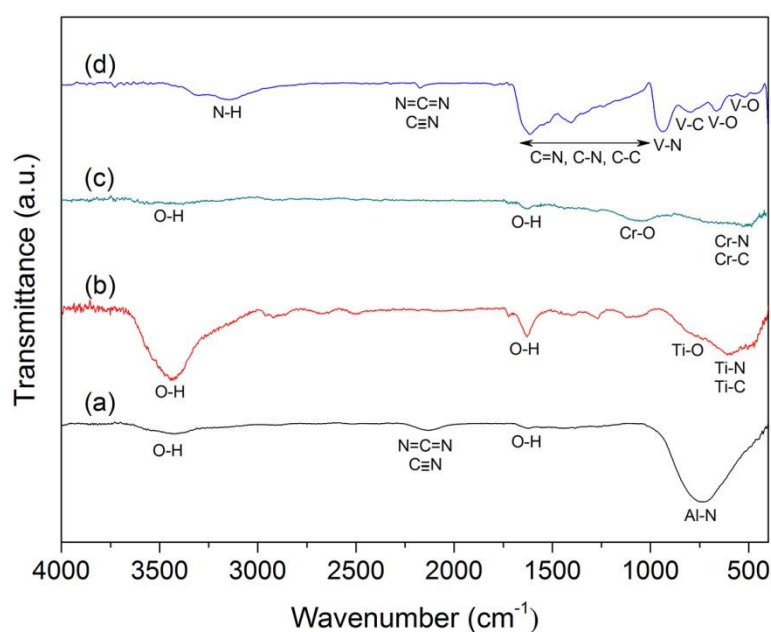

Fig. 2. FTIR spectra of the a) Al-M, b) Ti-M, c) Cr-M and d) V-M powder mixtures milled for 6, 30, 84 and 30 h, respectively.

To evaluate the chemical bonding states in the milling products and other CN-containing by-products, further characterization was conducted by XPS analysis (Fig. 3). For this, the obtained N1s and C1s spectra were first deconvoluted using Gaussian components, then, the chemical structure of the by-products was inferred from the XPS data, as schematically displayed in Fig. 3. As seen, all deconvoluted N1s spectra show a major peak at 396-397.3 eV assigned to the corresponding metal nitride N–M (M denotes to the metals including Al, Ti, Cr and V) [44]. The other three peaks in N1s spectra positioned at 397.9-398.6 eV, 399.2-399.7 eV and 400.3-400.9 eV are attributed to N–M–O (or C–N=C, pyridinic N), NH_x (or N–(C)$_3$, tertiary N) and M–N–O (or graphitic N), respectively [45-48], mainly resulting from surface oxidation of nitrides and/or formation of CN_x species. According to the Fig. 3a, the weak peak at 395.1 eV associated with AlN N1s spectrum is ascribed to N-N bonded defects on the surface of AlN, which originates from the nitrogen atoms with a coordination number of less than four and/ or the incomplete layer formation [45]. Moreover, the strong peak at 395.6 eV in Fig. 3d is attributed to N_x–Ti or N–Ti–O bonds caused by the nitrogen deficiency and/ or the surface oxidation [49, 50].

The major C1s peak is corresponding to sp^2 hybridized C–C bonds in graphite-like carbon [48] assumed to be from the formation of a carbonaceous by-product in all the samples (C1 spectra and schematics in Fig. 3) and is used for charge calibration (284.5 eV). The absence of carbonaceous phase in the XRD patterns, however, indicates to the non-crystalline characteristic of this phase. In the deconvoluted C1s spectra, the other peaks at the range of 285-291 eV are mainly attributed to C–OH (285.8 eV), N–C=N or C=O (287.7 eV), C–C=O (289.5 eV) and O–C=O (290.6 eV) [51] which confirms the simultaneously incorporation of nitrogen and oxygen atoms in the resulted carbon structures. The origin of the oxygen bonds comes from surface contamination of the samples. More specifically, in the case of V-M milled products, the N1s and C1s spectra illustrate the strong components at 398.6 eV (C–

N=C), 399.6 eV (N–$(C)_3$ and H_2N–C), 400.6 eV (graphitic N), 284.3 eV (sp^2 C–C), 286.3 eV (sp^2 C=N) and 287.9 eV (sp^3 C–N) which are the characteristic features of graphitic carbon nitride (CN_x), as reported in literature (the schematic illustration in Fig. 3i) [51, 52]. This interpretation is in good agreement with the strong bands observed at 1000-1720 cm^{-1} in the corresponding IR spectrum (Fig. 2d), confirming the incorporation of nitrogen in the carbonaceous phase. The existence of CN_x in the final product is resulted from the synthesis of carbide-based $V_2C_xN_{1-x}$ phase, as inferred from XRD analysis. Indeed, because of relative tendency to the formation of carbide phase, the vanadium precursor is partially consumed for the formation of $V_2C_xN_{1-x}$, leading to the presence of excess nitrogen incorporated in the carbonaceous phase.

The weak peak observed only in C1s spectra of Cr-M, Ti-M and V-M (not appeared in C1s spectrum of Al-M) milled systems at 281.6-282.6 eV is ascribed to the corresponding C-M bond (metal carbide) [53]. It is noteworthy to mention that nitrides, in general, are thermodynamically more favourable than carbides. To the best of our knowledge, transition metals such as Ti, Cr and V are known as strong carbide stabilizer elements which readily form carbides during various synthesis processes [17, 54]. Therefore, one may conclude that under the vigorous milling conditions, the elemental Ti, Cr and V powders simply react with both C and N atoms of organic precursor which in turn, form thermodynamically stable metal carbonitrides (MCNs). That's while Al preferably reacts with N atoms, leading to the formation of AlN instead of thermodynamically less stable Al_4C_3 and AlCN phases. From XPS results, x value in MC_xN_{1-x} is found to be about 0.05 which substantiates the formation of nitrogen-rich MCN phase.
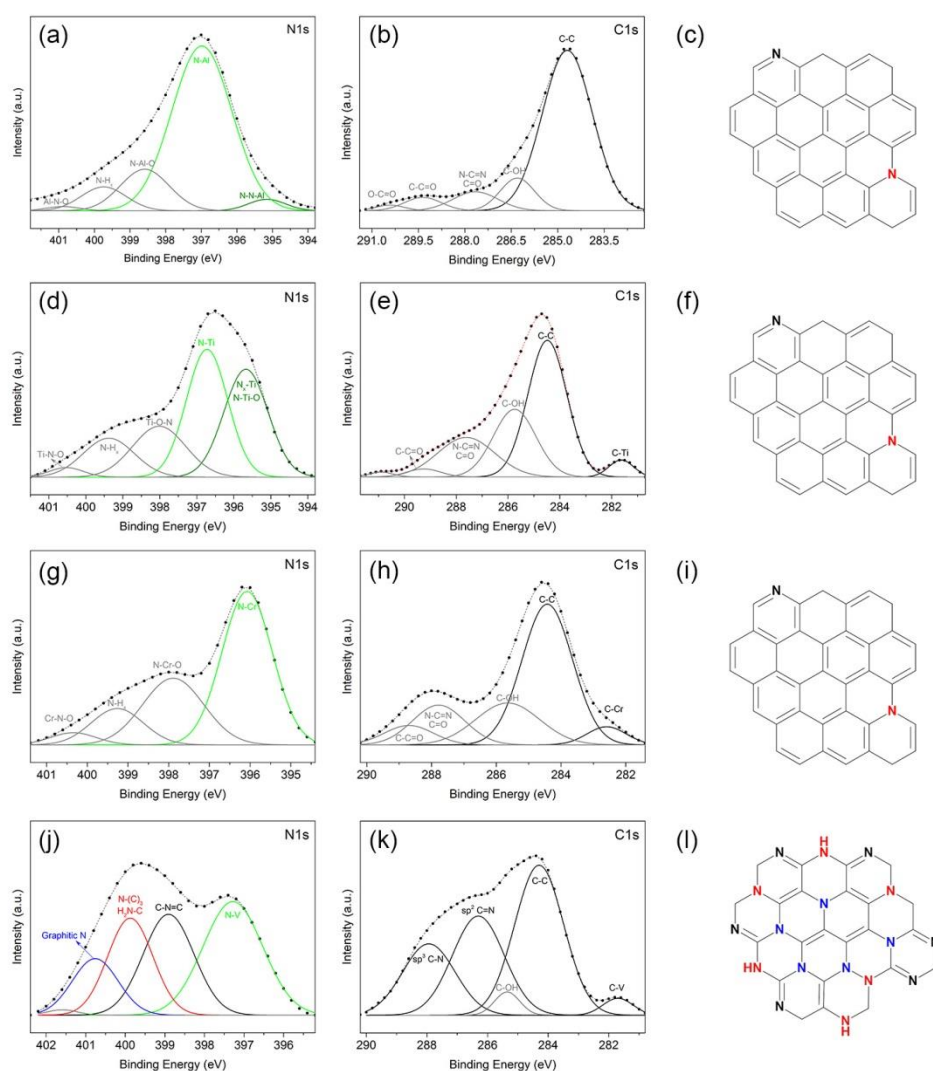
Fig. 3. Deconvoluted N1s and C1s spectra, and schematic chemical representation of the corresponding by-product for the (a-c) Al-M, (d-f) Ti-M, (g-i) Cr-M and (j-l) V-M powder mixtures milled for 6, 30, 84 and 30 h, respectively. The spectral components are indicated by solid lines, their sum by dashed lines and the experimental spectrum by dots.

Fig. 4 provides typical SEM images of the synthesized metal nitride and carbonitride at two different magnifications. The images demonstrate that the powder particles are highly aggregated into irregular shapes. High magnification SEM images confirm that the particle surfaces are structured in nanometer while mostly comprised of particles with sizes less than 100 nm, as corroborated by the XRD analyses (Fig. 1 and Table 1). However, comparing the

13

SEM images demonstrate the formation of large granules in Cr-M milled powder than the other synthesized products. This could be explained by the intrinsic ductility of fine CrC_xN_{1-x} particles, which aggregate to form large granules during the frequent fracture and cold welding of particles upon the milling process [55].

The SEM images and corresponding EDX mapping analyses of the milled powders in Fig. S3 demonstrate the uniform distribution of C, N and M (Al, Ti, Cr and V) elements in the powders. In Fig. S3a, the EDX maps of Al and N are originated from AlN particles. The origin of the C EDX maps in all the samples mainly arises from the carbonaceous by-product fabricated during the mechanochemical process, as confirmed by C1s spectra in XPS analyses. More specifically, the origin of C and N EDX maps in Fig. S3c is parttialy because of the formation of the CN_x networks as the main by-product in this sample.

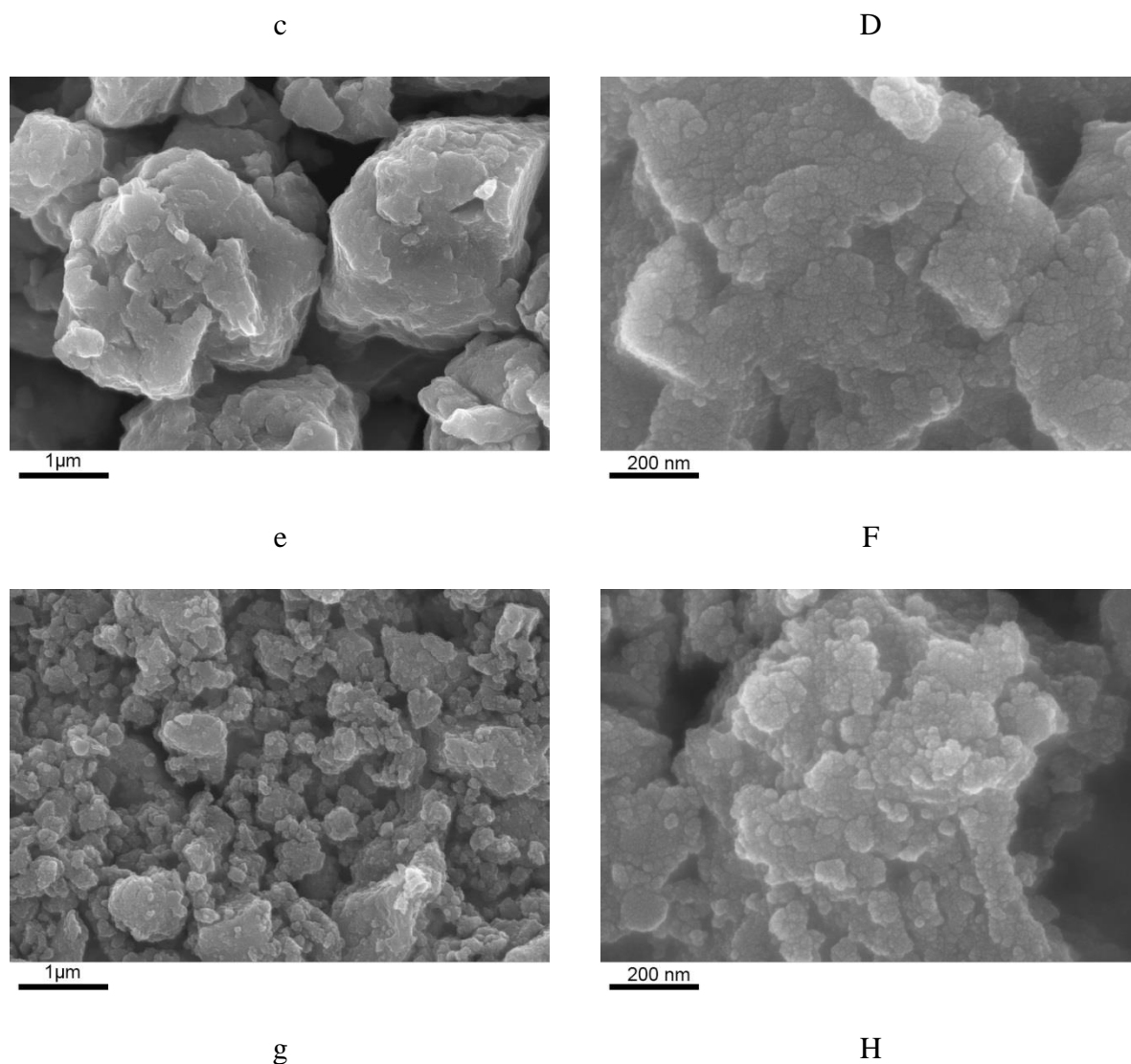
a

B

c

D

1μm

200 nm

e

F

1μm

200 nm

g

H
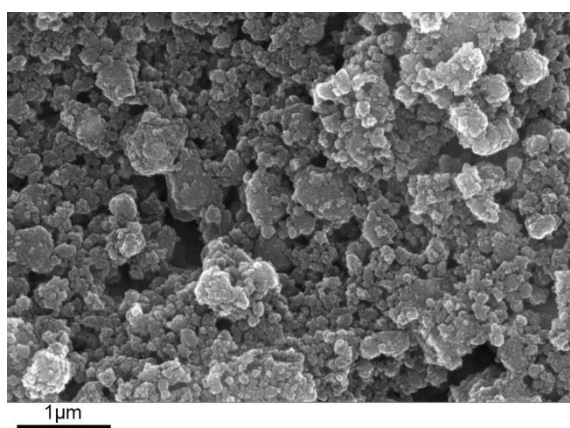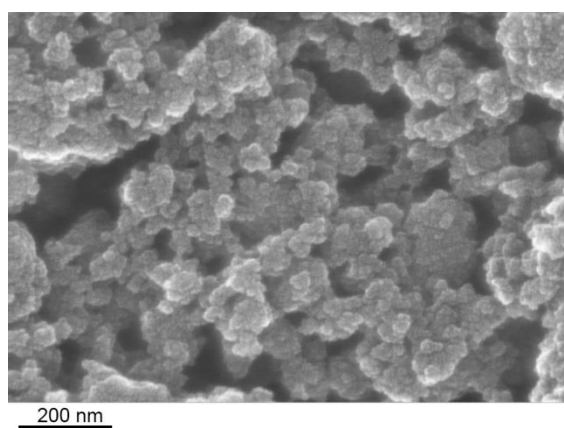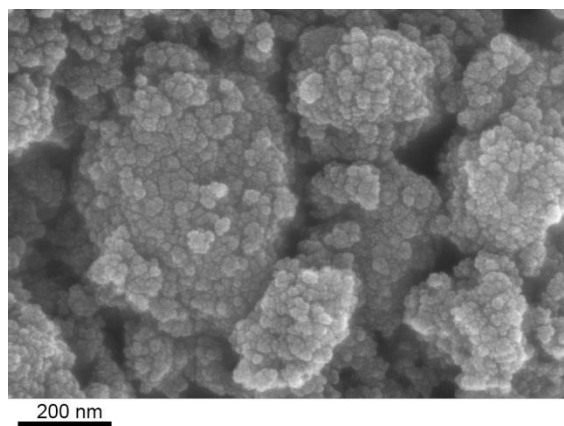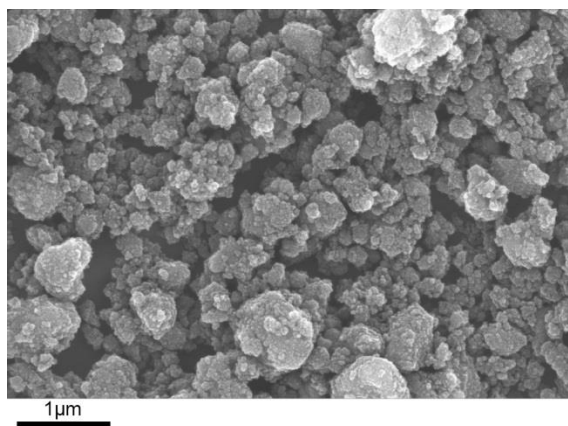
Fig. 4. Typical SEM images of a,b) Al-M, c, d) Ti-M, e, f) Cr-M and g, h) V-M powder mixtures milled for 6, 30, 84 and 30 h, respectively, prepared at different magnifications.

The above-mentioned results introduce a simple and cost-effective mechanochemical route for the synthesis of nanostructured MNs and MCNs. To propose the mechanism underlying this synthetic route, the reaction intermediates need to be well identified. Satisfying this demand, recently a detailed theoretical and experimental study was performed to characterize the intermediates in Al-M milling system [27]. The results revealed that melamine is polymerized at the intermediate stages of milling which leads to the formation of the CN_x network. This CN_x phase is potentially effective to interact with Al, resulting in the formation

of AlN by further milling. Our recent observations implied that this hypothesis could be feasibly extended to the other carbonitrides prepared in the current work. To achieve this purpose, in each milling system, the process was interrupted at the time exactly prior to the reaction initiation (intermediate stages), as inferred from the XRD results in Fig. S2. Afterwards, the FTIR spectra were collected from intermediates in each milling system (Fig. 5). For comparison, the FTIR spectrum of the as-received melamine is also provided (Fig. 5a).
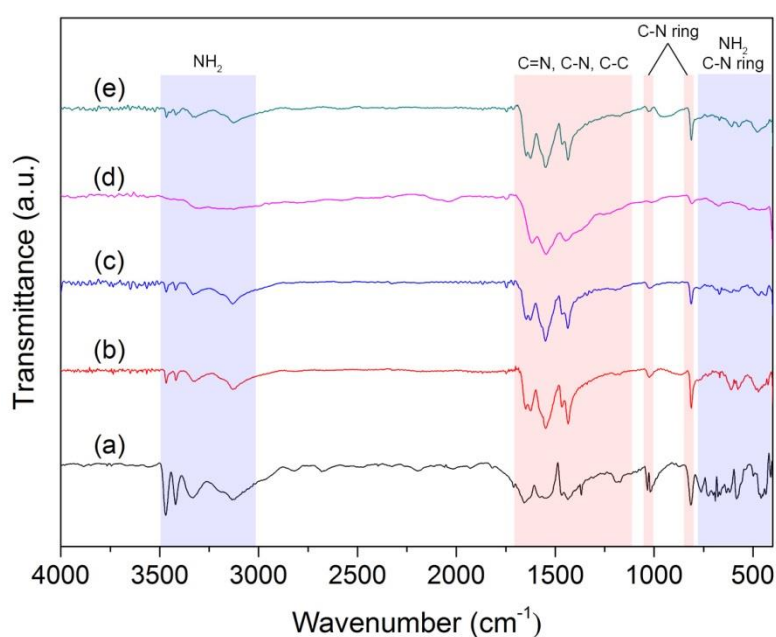

Fig. 5. FTIR spectra of a) as-received melamine and milled b) Al-M c) Ti-M d) Cr-M and e) V-M powder mixtures for 4, 20, 16 and 72 h, respectively.

The IR spectrum of melamine presents the strong transmittance peaks at 3000-3500 cm^{-1} and 1600-1650 cm^{-1} which correspond to the stretching vibration and bending modes of the amine groups, respectively. The peaks appeared in the range of 1100-1600 cm^{-1} are attributed to the C–N and C=N stretching vibration modes of the triazine ring. The bands observed at about 450-1050 cm^{-1} are assigned to the C–NH$_2$ along with the ring vibrations. The existence of signals at 814 cm^{-1} and 1027 cm^{-1} respectively point to the out-of-plane bending and

breathing modes of the triazine ring. Contrary to melamine, the peak intensities assigned to the NH_2 groups in the IR spectra of the milling intermediates (Fig. 5b-e) exhibit a significant reduction which obviously refers to the diammoniation of melamine. On the other hands, the fairly strong peaks located in the range of 1100-1600 cm^{-1} are attributed to the C–N and C=N vibrations as a result of the existence of N=C–N ring skeleton in the intermediates. A rational explanation for these observations could be the simultaneously deammoniation of melamine at the intermediate stages of milling followed by the polymerization of molecules and the formation of short range CN_x networks. This hypothesis is corroborated by our previous findings on the Al-M milling system [27] and the XPS results presented in the current investigation (Fig. 3c).

Based on the aforementioned results, the overall reaction mechanism is deduced, as schematically illustrated in Fig. 6. At the first stages of milling, deammoniation of melamine occurs in the presence of metallic elements. Simultaneously, nitrogen atoms of the broken amine groups gradually diffuse into the metal structure. The melamine radicals, then, merge to form a thermodynamically more stable CN_x phase [8]. Dependent on the stability of the corresponding metal nitride and carbide, C and/or N atoms are detached from the CN_x domain to diffuse into the metal structure. The diffusion proceeds until the metal structure reaches up to the solid solubility limit, in which further diffusion is allowed by the conversion of metallic structure to the corresponding MN or MCN phase. In the case of weak carbide former elements such as Al, the nitride (AlN) is the exclusive intermetallic structure fabricated, whereas, the conjugated C atoms form a carbonaceous by-product. In contrary, when the strong carbide formers such as Ti, Cr and V are used, the carbon atoms partially participate in the nitridation reaction which in turn, mainly forms a carbonitride structure together with a heterogeneous carbon phase. Moreover, in the case of VCN sample, as mentioned, the formation of a carbon rich phase ($V_2C_xN_{1-x}$) causes the incomplete nitridation

process. Consequently, besides the fabrication of VC_xN_{1-x} and $V_2C_xN_{1-x}$ phases, the synthesis of a CN_x phase is also expected. According to the findings, one may conclude that the final product in the current mechanochemical process can be altered depend on the milling time, type of metallic precursor and metal/melamine ratios, leading to the synthesis of wide variety of nanostructures including MNs, MCNs and many multicomponent systems such as MCN-CN_x composites.
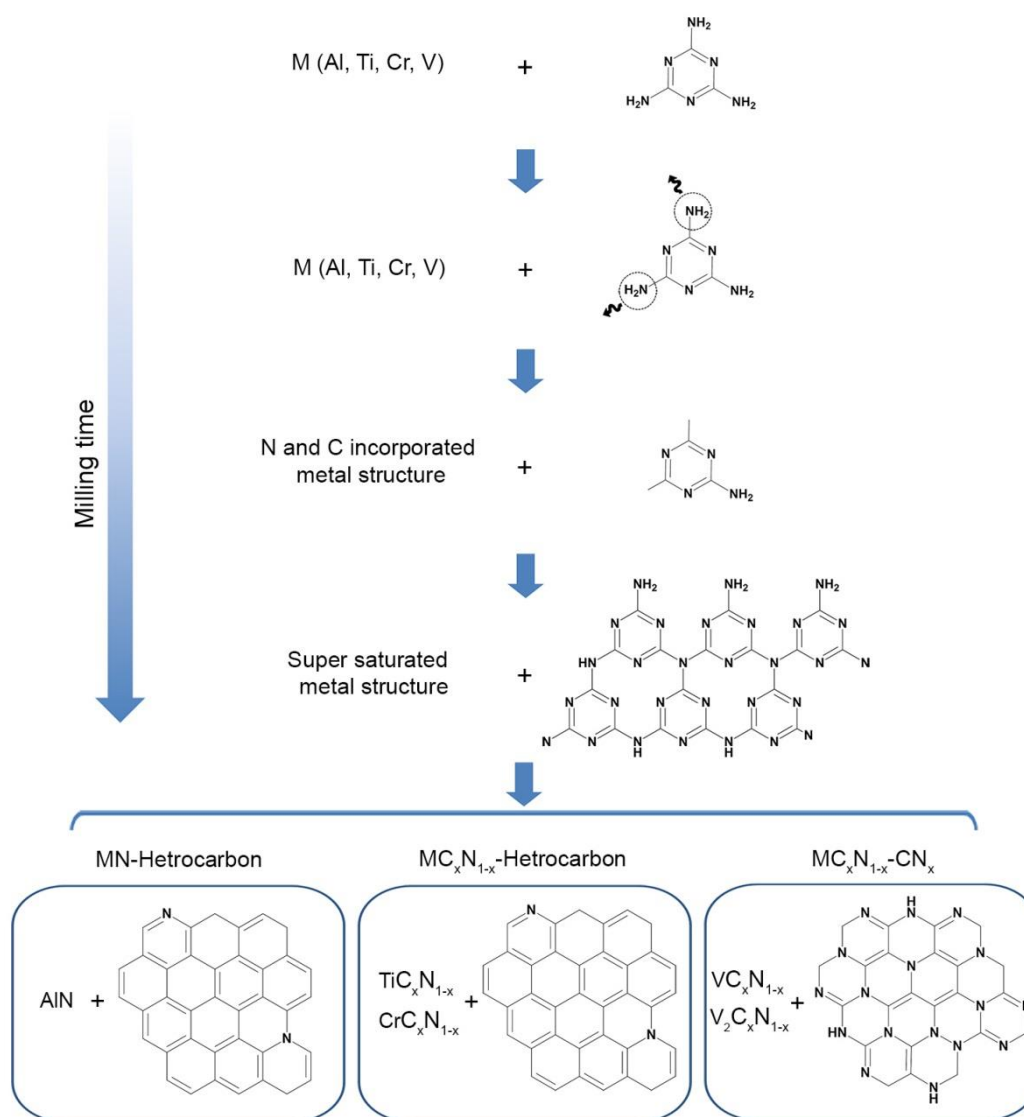

Fig. 6. The proposed reaction pathway for the mechanochemical reaction of various metals with melamine.

To corroborate the proposed reaction scheme shown in Fig. 6, *ab initio* density functional theory (DFT) calculations were performed (computational details are given in the SI) for four metals: Al (III), Ti(IV), V(V), and Cr(III). We considered the pure metals doped with either C or N, and a nitride and carbide form also doped with C and N, respectively. The super-cells were chosen to give rise to dopant concentrations of about 1-3%. This is slightly lower than the experimental dopant concentration (~5%), but it is expected not to influence the qualitative picture as was observed in other work on doped materials.[5,6] To compare the total energies of the systems we calculated the formation energy as:

$$E_f = E_{sys} - \sum_i N_i E_i \ ,$$

with E_{sys} the total energy of the system under study, N_i the number of atoms of a specific species (C, N, Metal=Al, Ti, V) and E_i the chemical potential of that atomic species (graphene and N_2 gas were used as the reference systems). In addition, also the defect formation energy was calculated as:

$$E_d = E_{sys} - N_{cell} E_{host} - \sum_i \Delta N_i E_i \ ,$$

with N_{cell} the size of the super cell used (18 for a 3x3x2 super cell), E_{host} the total energy for one unit cell of the host material, and ΔN_i the change in number of atoms of a specific species (either 1 or 0).

The resulting energies are presented in Table 2. For each of the metals, it was found that both the metal-carbide and metal-nitride stabilize the system, with the metal-nitride being most stable. For the chromium, two carbides were investigated: CrC and $Cr_{23}C_6$, of which only the latter is stable in comparison to the metal, a first indication that only low C concentrations should be expected in Cr. In overall, in the case of pure metal, either interstitial C or N

doping is more favourable than substitutional one, while for nitride and carbide the substitutional doping is more stable.

Table 2. Associated formation energies calculated for N and C incorporations in four distinct metals, nitrides and carbides.

	Metal			Nitride			Carbide		
	System	E_f (eV)	E_d (eV)	System	E_f (eV)	E_d (eV)	System	E_f (eV)	E_d (eV)
Aluminum	Al	0.000	na	AlN	-1.364	na	Al_4C_3	-0.081	na
	Al:N Sub	0.100	-5.188	AlN:C Sub	-1.297	4.818	Al_4C_3:N Sub T	-0.098	-1.443
	Al:N Int T	-0.023	-9.162	AlN:C Int H	-1.253	6.737	Al_4C_3:N Sub H	-0.083	-0.182
	Al:N Int O	0.001	-8.370	AlN:C Int T	-1.258	6.394	Al_4C_3:N Int H	-0.027	4.522
	Al:C Sub	0.132	4.209				Al_4C_3:N Int C	-0.060	1.659
	Al:C Int T	0.056	1.855						
	Al:C Int O	0.045	1.492						
Titanium	Ti	0.000	na	TiN	-1.718	na	TiC	-0.824	na
	Ti:N Sub	0.070	2.523	TiN:C Sub	-1.694	1.547	TiC:N Sub	-0.858	-2.151
	Ti:N Int H	-0.103	-3.800	TiN:C Int	-1.575	7.602	TiC:N Int	-0.732	5.161
	Ti:N Int C	-0.059	-2.193						
	Ti:C Sub	0.076	2.748						
	Ti:C Int H	-0.043	-1.584						
	Ti:C Int C	0.012	0.455						
Vanadium	V	0.000	na	VN	-0.944	na	VC	-0.407	na
	V:N Sub	0.034	1.809	VN:C Sub	-0.929	0.984	VC:N Sub	-0.426	-1.237
	V:N Int	-0.049	-2.716	VN:C Int	-0.834	6.247	VC:N Int	-0.316	5.495
	V:C Sub	0.040	2.175						
	V:C Int	-0.014	-0.775						
Chromium	Cr	0.000	na	CrN	-0.338	na	CrC	0.160	Na
	Cr:N Sub	0.065	3.522	CrN:C Sub	-0.360	-1.386	CrC:N Sub	0.151	-0.568
	Cr:N Int	0.004	0.220	CrN:C Int	-0.245	5.741	CrC:N Int	0.242	5.472
	Cr:C Sub	0.060	3.244				$Cr_{23}C_6$	-0.086	na
	Cr:C Int	0.025	1.387				$Cr_{23}C_6$:N Sub	-0.088	-0.259
							$Cr_{23}C_6$:N Int	-0.067	2.091

In case of Al, aluminium-carbide appears to be only barely more stable than Al itself. Furthermore, the calculated defect formation energies show it to be energetically very

unfavourable to dope Al with C, while N doping is shown to be very favourable. In addition, the defect formation energies for Al_4C_3 and AlN show that substitution of a C atom in Al_4C_3 will stabilize the system significantly, while substitution of a N atom in AlN will destabilize the system. This provides a global picture of N being incorporated into the Al lattice, initially as interstitial defects, which were shown to cluster [27], transforming the material into AlN. If Al_4C_3 phases are present, N substitution will quickly transform these phases into AlN, pushing C out of the "Al metal".

In contrast to Al, both C and N (interstitial) defects are stable in Ti. In addition, also both titanium nitride and carbide are stable, an indication that the defects will cluster. As the E_d values for doping in Ti are smaller than those obtained for Al, the formation of the nitrides and carbides is expected to be slower than was the case for AlN. This means that at the same milling conditions a longer milling time is required for TiC_xN_{1-x} synthesis (30 h) in comparison with AlN (6 h). Since the formation energies of doped and undoped carbide and nitride are favourable, mixed TiC_xN_{1-x} compounds are also expected to be formed as a result of co-doping of N and C, with the former having the higher concentration. The calculated defect formation energies for the doped nitride and carbide show a picture similar as was seen for Al; C-doping of the nitride is unfavourable, while substitutional N doping of the carbide is energetically favourable, leading to mixed compounds with higher N concentration. Additionally, this also indicates that, during extended ball-milling, the carbide phases (which should be much more abundant than for the Al case) are expected to transform into the nitride form. As a result, one may expect to see a gradual decline in carbide phases over the duration of the synthesis.

Also for the V metal, the C and N (interstitial) defects are stable and have favourable defect formation energies. As both the nitride and carbide are stable compounds, defects will cluster to form both VC and VN phases. Also the doped nitrides and carbides are stable (E_f <0)

indicating mixed VC_xN_{1-x} compounds should be expected. The defect formation energies for the carbide and nitride show the same qualitative picture as was the case for Ti, again indicating that C can be substituted by N. However, as the difference in formation energy of the nitride and carbide is smaller than was the case for Ti, a relatively larger fraction of carbide phase is to be expected formed during the initial phases of synthesis. As a result, the carbide-based $V_2C_xN_{1-x}$ phase is expected to be synthesized.

The Cr metal behaves slightly different. In contrast to the other metals, neither C nor N defect is favourable. Also the carbide (CrC) is unfavourable and only at much lower C concentration the carbide ($Cr_{23}C_6$) is marginally stable. The nitride on the other hand is stable, albeit with the lowest formation energy of the set of metals investigated. Combined with the unfavourable N-doping of Cr this indicates that the nitride-formation process should be much slower than for the other metals (84 h milling time is required). Another interesting difference is the fact that substitutional C doping of the nitride is energetically favourable. So although the incorporation of C in pure Cr is not favoured, it becomes possible in CrN, allowing for the formation of CrC_xN_{1-x} compounds. Full transformation into a carbide will be counteracted by the fact that similar as for the other metals, N substitutional doping of the carbide is also favourable. As a result one should expect to find CrC_xN_{1-x} mixed compounds. Note, however, that although both Ti and Cr are expected to give rise to mixed compounds, the mechanism for their formation differs significantly. Where the Ti mixed compounds originate from initial co-doping and transformation of carbide into nitride, the Cr mixed compounds originate from the initial formation of a CrN which is then doped with C.

4. Conclusions

A simple, low cast and versatile mechanochemical process was proposed for synthesis of various nanostructured metal nitrides and carbonitrides including AlN, TiC_xN_{1-x}, CrC_xN_{1-x},

and VC_xN_{1-x} /$V_2C_xN_{1-x}$. The process opens an avenue for the facile synthesis of wide variety of promising MN, MCN nanostructures and their complexes such as MCN-CN_x nanocomposites through the solid –state reaction of melamine with metallic elements under the vigorous mechanical forces. It was found that the reaction initiates with the deammoniation of melamine molecules and diffusion of N and C atoms to the metal structure following with the polymerization and formation of conjugated C-N heterocycles at the intermediate stages of milling. The supersaturated metallic structure, then, reacts with C and N atoms of the CN_x intermediate phase and transforms to MN or MCN depends on the total energy of system and the defect formation energy of corresponding carbide and nitride. For Ti, Cr and V, in which both nitride and carbide are favourable, a mixed carbonitride phase is formed while in case of Al, only nitride (AlN) is stable. An amorphous heterocarbon phase was also found to be present in all samples. For V-M milling system which the carbide-based $V_2C_xN_{1-x}$ phase is formed, there is a lack of sufficient metallic vanadium for nitridation completion. Hence, intact N atoms incorporate in the carbonaceous phase to form a CN_x phase besides the MCN structure (VC_xN_{1-x} /$V_2C_xN_{1-x}$).

6. References

[1]   M.T. Hardy, D.F. Feezell, S.P. DenBaars, S. Nakamura. Group III-nitride lasers: a materials perspective, Materials Today 14 (2011) 408-415.

[2]   M. Kneissl, T. Kolbe, C. Chua, V. Kueller, N. Lobo, J. Stellmach, A. Knauer, H. Rodriguez, S. Einfeldt, Z. Yang, N.M. Johnson, M. Weyers. Advances in group III-nitride-based deep UV light-emitting diode technology, Semiconductor Science and Technology 26 (2011) 014036.

[3]   H. Klemm. Silicon nitride for high-temperature applications, Journal of the American Ceramic Society 93 (2010) 1501-1522.

[4]   R. Bayón, A. Igartua, X. Fernández, R. Martínez, R.J. Rodríguez, J.A. García, A. de Frutos, M.A. Arenas, J. de Damborenea. Corrosion-wear behaviour of PVD Cr/CrN multilayer coatings for gear applications, Tribology International 42 (2009) 591-599.

[5]   J. Zhang, Q. Xue, S. Li. Microstructure and corrosion behavior of TiC/Ti(CN)/TiN multilayer CVD coatings on high strength steels, Applied Surface Science 280 (2013) 626-631.

[6]   T. Huang, S. Mao, G. Zhou, Z. Wen, X. Huang, S. Ci, J. Chen. Hydrothermal synthesis of vanadium nitride and modulation of its catalytic performance for oxygen reduction reaction, Nanoscale 6 (2014) 9608-9613.

[7]   Z. Zhao, Y. Dai, J. Lin, G. Wang. Highly-Ordered Mesoporous Carbon Nitride with Ultrahigh Surface Area and Pore Volume as a Superior Dehydrogenation Catalyst, Chemistry of Materials 26 (2014) 3151-3161.

[8]   Y. Wang, X. Wang, M. Antonietti. Polymeric Graphitic Carbon Nitride as a Heterogeneous Organocatalyst: From Photochemistry to Multipurpose Catalysis to Sustainable Chemistry, Angewandte Chemie International Edition 51 (2012) 68-89.

[9]   B. Mazumder, A.L. Hector. Synthesis and applications of nanocrystalline nitride materials, Journal of Materials Chemistry 19 (2009) 4673-4686.

[10]   B.M. Eick, J.P. Youngblood. Carbothermal reduction of metal-oxide powders by synthetic pitch to carbide and nitride ceramics, J Mater Sci 44 (2009) 1159-1171.

[11]   A. Paseuth, S. Shimada. Synthesis and mechanism of manosized AlN from an aluminum oleic emulsion using carbothermal reduction at low temperatures, Journal of the American Ceramic Society 91 (2008) 1129-1134.

[12]   S. Colque, P. Grange. Proposal for a new mechanism for the transformation of alumina into aluminiurn nitride, Journal of Materials Science Letters 13 (1994) 621-622.

[13]   J.-K. Kim, W.-S. Jung. Nitridation of δ-alumina to aluminum nitride under a flow of ammonia and its mechanism, Journal of the Ceramic Society of Japan 119 (2011) 351-354.

[14]   H. Zhao, M. Lei, X. Chen, W. Tang. Facile route to metal nitrides through melamine and metal oxides, Journal of Materials Chemistry 16 (2006) 4407-4407.

[15]   B.V. Lotsch, W. Schnick. Thermal conversion of guanylurea dicyanamide into graphitic carbon nitride via prototype CNx precursors, Chemistry of Materials 17 (2005) 3976-3982.

[16]   Y. Du, M. Lei, H. Yang. Facile solid-state synthesis route to metal nitride nanoparticles, Journal of materials science & technology 24 (2008) 737-741.

[17]   C. Giordano, M. Antonietti. Synthesis of crystalline metal nitride and metal carbide nanostructures by sol–gel chemistry, Nano Today 6 (2011) 366-380.

[18]   V.V. Zyryanov. Mechanochemical synthesis of complex oxides, Russian Chemical Reviews 77 (2008) 105.

[19]   J. Huot, D.B. Ravnsbæk, J. Zhang, F. Cuevas, M. Latroche, T.R. Jensen. Mechanochemical synthesis of hydrogen storage materials, Progress in Materials Science 58 (2013) 30-75.

[20]   S.L. James, C.J. Adams, C. Bolm, D. Braga, P. Collier, T. Friscic, F. Grepioni, K.D.M. Harris, G. Hyett, W. Jones, A. Krebs, J. Mack, L. Maini, A.G. Orpen, I.P. Parkin,

W.C. Shearouse, J.W. Steed, D.C. Waddell. Mechanochemistry: opportunities for new and cleaner synthesis, Chemical Society Reviews 41 (2012) 413-447.

[21]   V. León, A.M. Rodriguez, P. Prieto, M. Prato, E. Vázquez. Exfoliation of graphite with triazine derivatives under ball-milling conditions: preparation of few-layer graphene via selective noncovalent interactions, ACS Nano 8 (2013) 563-571.

[22]   I.-Y. Jeon, H.-J. Choi, S.-M. Jung, J.-M. Seo, M.-J. Kim, L. Dai, J.-B. Baek. Large-Scale Production of Edge-Selectively Functionalized Graphene Nanoplatelets via Ball Milling and Their Use as Metal-Free Electrocatalysts for Oxygen Reduction Reaction, Journal of the American Chemical Society 135 (2012) 1386-1393.

[23]   M.A. Roldan, V. López-Flores, M.D. Alcala, A. Ortega, C. Real. Mechanochemical synthesis of vanadium nitride, Journal of the European Ceramic Society 30 (2010) 2099-2107.

[24]   E.S. Caballero, J. Cintas, F.G. Cuevas, J.M. Montes, J.M. Gallardo. A new method for synthetizing nanocrystalline aluminium nitride via a solid–gas direct reaction, Powder Technology 287 (2016) 341-345.

[25]   P. Li, S. Xi, J. Zhou. Phase transformation and gas–solid reaction of Al2O3 during high-energy ball milling in N2 atmosphere, Ceramics International 35 (2009) 247-251.

[26]   A. Calka, J.I. Nikolov. Direct synthesis of AlN and Al-AlN composites by room temperature magneto ball milling: the effect of milling condition on formation of nanostructures, Nanostructured Materials 6 (1995) 409-412.

[27]   S.A. Rounaghi, H. Eshghi, S. Scudino, A. Vyalikh, D.E.P. Vanpoucke, W. Gruner, S. Oswald, A.R. Kiani Rashid, M. Samadi Khoshkhoo, U. Scheler, J. Eckert. Mechanochemical route to the synthesis of nanostructured Aluminium nitride, Scientific Reports 6 (2016) 33375.

[28]   G. Kresse, D. Joubert. From ultrasoft pseudopotentials to the projector augmented-wave method, Physical Review B 59 (1999) 1758-1775.

[29]   P.E. Blöchl. Projector augmented-wave method, Physical Review B 50 (1994) 17953-17979.

[30]   J.P. Perdew, K. Burke, M. Ernzerhof. Generalized Gradient Approximation Made Simple, Phys. Rev. Lett. 77 (1996) 3865-3868.

[31]   H.J. Monkhorst, J.D. Pack. Special points for Brillouin-zone integrations, Physical Review B 13 (1976) 5188-5192.

[32]   K.-I. Kim, S.-C. Choi, J.-H. Kim, W.-S. Cho, K.-T. Hwang, K.-S. Han. Synthesis and characterization of high-purity aluminum nitride nanopowder by RF induction thermal plasma, Ceramics International 40 (2014) 8117-8123.

[33]   S. Sedira, S. Achour, A. Avci, V. Eskizeybek. Physical deposition of carbon doped titanium nitride film by DC magnetron sputtering for metallic implant coating use, Applied Surface Science 295 (2014) 81-85.

[34]   N.I. Fainer, A.N. Golubenko, Y.M. Rumyantsev, V.G. Kesler, E.A. Maksimovskii, F.A. Kuznetsov. Preparation of nanocrystalline titanium carbonitride coatings using Ti(N(Et)2)4, Glass Phys Chem 37 (2011) 322-329.

[35]   H. Zhang, X. Lv, Y. Li, Y. Wang, J. Li. P25-Graphene Composite as a High Performance Photocatalyst, ACS Nano 4 (2010) 380-386.

[36]   H. Makoto, U. Yasuhiro, S. Tsuneo, J. Weihua, G. Constantin, Y. Kiyoshi. Characteristics of CrN Films Prepared by Pulsed Laser Deposition, Japanese Journal of Applied Physics 40 (2001) 1052.

[37]   H. Sun, L. Wang, D. Chu, Z. Ma, A. Wang. Synthesis of porous Cr2O3 hollow microspheres via a facile template-free approach, Materials Letters 140 (2015) 35-38.

[38]   E.F. de Souza, C.A. Chagas, T.C. Ramalho, V. Teixeira da Silva, D.L.M. Aguiar, R.S. Gil, R.B. de Alencastro. A Combined Experimental and Theoretical Study on the Formation of Crystalline Vanadium Nitride (VN) in Low Temperature through a Fully Solid-State Synthesis Route, The Journal of Physical Chemistry C 117 (2013) 25659-25668.

[39]   T. Radhika, S. Sugunan. Vanadia supported on ceria: Characterization and activity in liquid-phase oxidation of ethylbenzene, Catalysis Communications 8 (2007) 150-156.

[40]   I.L. Botto, M.B. Vassallo, E.J. Baran, G. Minelli. IR spectra of VO2 and V2O3, Materials Chemistry and Physics 50 (1997) 267-270.

[41]   Q.X. Guo, Q. Yang, C.Q. Yi, L. Zhu, Y. Xie. Synthesis of carbon nitrides with graphite-like or onion-like lamellar structures via a solvent-free route at low temperatures, Carbon 43 (2005) 1386-1391.

[42]   S. Yang, Y. Gong, J. Zhang, L. Zhan, L. Ma, Z. Fang, R. Vajtai, X. Wang, P.M. Ajayan. Exfoliated Graphitic Carbon Nitride Nanosheets as Efficient Catalysts for Hydrogen Evolution Under Visible Light, Advanced Materials 25 (2013) 2452-2456.

[43]   P. Niu, L. Zhang, G. Liu, H.-M. Cheng. Graphene-like carbon nitride nanosheets for improved photocatalytic activities, Advanced Functional Materials 22 (2012) 4763-4770.

[44]   I. Bertóti. Characterization of nitride coatings by XPS, Surface and Coatings Technology 151–152 (2002) 194-203.

[45]   L. Rosenberger, R. Baird, E. McCullen, G. Auner, G. Shreve. XPS analysis of aluminum nitride films deposited by plasma source molecular beam epitaxy, Surface and Interface Analysis 40 (2008) 1254-1261.

[46]   H. Liu, D.C. Bertolet, J.W. Rogers Jr. The surface chemistry of aluminum nitride MOCVD on alumina using trimethylaluminum and ammonia as precursors, Surf. Sci. 320 (1994) 145-160.

[47]   N. Hellgren, R.T. Haasch, S. Schmidt, L. Hultman, I. Petrov. Interpretation of X-ray photoelectron spectra of carbon-nitride thin films: New insights from in situ XPS, Carbon 108 (2016) 242-252.

[48]   Z.-H. Sheng, L. Shao, J.-J. Chen, W.-J. Bao, F.-B. Wang, X.-H. Xia. Catalyst-Free Synthesis of Nitrogen-Doped Graphene via Thermal Annealing Graphite Oxide with Melamine and Its Excellent Electrocatalysis, ACS Nano 5 (2011) 4350-4358.

[49]   L.K. Randeniya, A. Bendavid, P.J. Martin, E.W. Preston. Photoelectrochemical and Structural Properties of TiO2 and N-Doped TiO2 Thin Films Synthesized Using Pulsed Direct Current Plasma-Activated Chemical Vapor Deposition, The Journal of Physical Chemistry C 111 (2007) 18334-18340.

[50]   C. Chen, H. Bai, C. Chang. Effect of Plasma Processing Gas Composition on the Nitrogen-Doping Status and Visible Light Photocatalysis of TiO2, The Journal of Physical Chemistry C 111 (2007) 15228-15235.

[51]   Y. Wang, Y. Shao, D.W. Matson, J. Li, Y. Lin. Nitrogen-doped graphene and its application in electrochemical biosensing, ACS Nano 4 (2010) 1790-1798.

[52]   J. Liu, T. Zhang, Z. Wang, G. Dawson, W. Chen. Simple pyrolysis of urea into graphitic carbon nitride with recyclable adsorption and photocatalytic activity, Journal of Materials Chemistry 21 (2011) 14398-14401.

[53]   J. Halim, K.M. Cook, M. Naguib, P. Eklund, Y. Gogotsi, J. Rosen, M.W. Barsoum. X-ray photoelectron spectroscopy of select multi-layered transition metal carbides (MXenes), Applied Surface Science 362 (2016) 406-417.

[54]   S. Gomari, S. Sharafi. Microstructural characterization of nanocrystalline chromium carbides synthesized by high energy ball milling, Journal of Alloys and Compounds 490 (2010) 26-30.

[55]   C. Real, M.A. Roldán, M.D. Alcalá, A. Ortega. Synthesis of Nanocrystalline

Chromium Nitride Powder by Mechanical Processing, Journal of the American Ceramic

Society 90 (2007) 3085-3090.